Density-Functional Study of Interfacial Properties of Colloid−Polymer Mixtures†

A. Moncho-Jordá,*,‡ J. Dzubiella,§ J. P. Hansen,§ and A. A. Louis§

Departamento de Física Aplicada, Universidad de Granada, Facultad de Ciencias, Campus Fuentenueva S/N, 18071 Granada, Spain, and Department of Chemistry, University of Cambridge, Lensfield Road, Cambridge CB2 1EW, United Kingdom

Received: September 14, 2004; In Final Form: November 4, 2004

Interfacial properties of colloid−polymer mixtures are examined within an effective one-component representation, where the polymer degrees of freedom are traced out, leaving a fluid of colloidal particles interacting via polymer-induced depletion forces. Restriction is made to zero-, one-, and two-body effective potentials, and a free energy functional is used that treats colloid excluded volume correlations within Rosenfeld's fundamental measure theory, and depletion-induced attraction within first-order perturbation theory. This functional allows a consistent treatment of both ideal and interacting polymers. The theory is applied to surface properties near a hard wall, to the depletion interaction between two walls, and to the fluid−fluid interface of demixed colloid−polymer mixtures. The results of the present theory compare well with predictions of a fully two-component representation of mixtures of colloids and ideal polymers (the Asakura−Oosawa model) and allow a systematic investigation of the effects of polymer−polymer interactions on interfacial properties. In particular, the wall surface tension is found to be significantly larger for interacting than for ideal polymers, whereas the opposite trend is predicted for the fluid−fluid interfacial tension.

I. Introduction

Mixtures of colloidal particles and nonadsorbing polymers dispersed in a solvent provide experimentalists and theoreticians with a very flexible model system to explore the statics and dynamics of phase transitions, including fluid−fluid demixing, crystallization, gelation, or glass transitions,[1] as well as the interfacial properties associated with phase coexistence. The flexibility of this model system stems from the fact that its properties can be easily tuned by varying, among others, the size ratio of the two components (e.g., by controlling the degree of polymerization), their concentrations, or the quality of the solvent that determines whether the polymer coils behave essentially like interacting self-avoiding walks (SAW), or more like ideal noninteracting polymers (under θ-solvent conditions).

More specifically, if, as will be done in this paper, one adopts an effective one-component representation (by tracing out the polymer degrees of freedom), the resulting effective interactions between the colloidal particles, obtained from the well-known depletion mechanism,[2] are easily tuned by varying the above physical parameters: the depth of the effective attraction between colloids is essentially controlled by the polymer concentration, whereas the range depends on the polymer size (radius of gyration). The resulting phase diagrams are very sensitive to changes in the depletion-induced pair potential between colloids.[3] Recent experimental[4] and theoretical[5,6] efforts have focused on interfacial and wetting properties of colloid−polymer mixtures, either near solid substrates (hard walls) or at fluid−fluid phase coexistence. The density profiles near a glass wall and the surface tension at fluid−fluid phase coexistence were measured[4] and very recently the first direct observation of capillary fluctuations at the fluid−fluid interface was reported.[7] Various versions of density functional theory (DFT) of inhomogeneous fluids have been used to determine the density profiles, adsorption, and surface tension of colloid−polymer mixtures near a hard wall, either in the one-component[8] or two-component[9,10] representations or at the phase-separated fluid−fluid interface.[11,12] Most of the theoretical work so far focused on mixtures of hard sphere colloids and ideal (noninteracting) polymers within the classic model of Asakura and Oosawa[13] and of Vrij[14] (the AO model), although some attempts have been made to extend the DFT calculations to the case of nonideal (interacting) polymer coils,[10,12] pointing to very significant differences between the two situations.

This paper presents a unified DFT description of wall−fluid and fluid−fluid interfaces within an effective one-component representation. The DFT theory is a perturbative one with respect to the polymer-induced depletion attraction between hard sphere colloids and applies to mixtures of colloids and noninteracting, as well as interacting, polymer coils. Apart from a systematic comparison of the density profiles and surface tensions obtained for these two cases, the present theory also leads to the first estimate of the depletion potential between two walls induced by colloid−polymer mixtures.

The paper is organized as follows. Section II briefly summarizes the effective one and two-component representations of colloid−polymer mixtures. The DFT formulation used in this paper is presented in section III. Results for colloid density profiles near a hard wall in the presence of ideal or interacting polymers are presented in section IV, whereas the resulting wall surface tension of the mixtures is calculated in section V. The depletion potential between hard walls, induced by colloid−polymer mixtures is described in section VI. The fluid−fluid interfacial properties calculated within the same DFT approximation are presented in section VII, and conclusions are drawn in section VIII.

† Part of the special issue "David Chandler Festschrift".

* To whom correspondence should be addressed. E-mail: moncho@ugr.es.
‡ Universidad de Granada.
§ University of Cambridge.

10.1021/jp045841x CCC: $30.25
Published on Web 02/01/2005

II. Effective One- and Two-Component Representations

Consider a binary mixture of N_c colloidal particles and N_p polymer coils in an external field (e.g., the confining field of a hard wall). The total Hamiltonian of the system may be written as

$$H = H_{cc} + H_{pp} + H_{cp} + \Phi_c + \Phi_p \tag{1}$$

where the colloid−colloid, polymer−polymer, and colloid−polymer terms H_{cc}, H_{pp}, and H_{cp} will be assumed to be sums of pair interactions between the centers of mass (CM)$\{\vec{R}_i\}$ ($1 \le i \le N_c$) and $\{\vec{r}_j\}$ ($1 \le j \le N_p$) of the colloids and polymers, respectively. Within this assumption, the individual monomer degrees of freedom of the polymer coils have been traced out, and the resulting effective pair potential between polymer CM's is a state-dependent free energy;[15] similarly the colloid−polymer pair potential is a state-dependent free energy resulting from a statistical average over monomer degrees of freedom for a fixed distance between the CM's of the two particles.[16] Hence,

$$H_{cc} = \sum_{i<j}^{N_c} v_{cc}(R_{ij})$$

$$H_{pp} = \sum_{i<j}^{N_p} v_{pp}(r_{ij})$$

$$H_{cp} = \sum_{i}^{N_c}\sum_{j}^{N_p} v_{cp}(|\vec{R}_i - \vec{r}_j|) \tag{2}$$

and

$$\Phi_c = \sum_{i}^{N_c} \varphi_c^0(\vec{R}_i) \qquad \Phi_p = \sum_{i}^{N_p} \varphi_p^0(\vec{r}_i) \tag{3}$$

where φ_c^0 and φ_p^0 are direct external interactions acting on colloidal particles and polymers, respectively. Note that $\varphi_p^0(\vec{r})$ is once more an effective potential acting on the polymer CM.

The colloid−colloid pair potential will henceforth always be considered to be of the hard sphere form. The AO model for noninteracting polymers further assumes that

$$v_{\alpha\beta}(r) = \begin{cases} \infty & r < \sigma_{\alpha\beta} \\ 0 & r > \sigma_{\alpha\beta}; \ \alpha, \beta = \text{c or p} \end{cases} \tag{4}$$

with $\sigma_{cc} = 2R_c$ (R_c being the colloidal radius), $\sigma_{pp} = 0$, and $\sigma_{cp} = R_c + R_p$, where R_p is the radius of gyration of the polymer coils. A generalization of Rosenfeld's fundamental measure theory (FMT) free energy functional for additive hard spheres[17] has been worked out for the nonadditive hard sphere mixture given by eq 4[18] and applied to colloid−polymer interfacial properties.[5,9]

An alternative approach is to trace out the polymer degrees of freedom to derive an effective Hamiltonian involving only the colloid degrees of freedom.[2,19] Within the semi-grand canonical ensemble, with fixed N_c and fixed chemical potential μ_p of the polymers (or equivalently, fixed number density ρ_p^r of the polymers in a reservoir), the effective Hamiltonian is

$$H_c^{eff} = H_{cc} + \Phi_c + \Omega \tag{5}$$

where Ω is the grand potential of the inhomogeneous fluid of polymers, which depends parametrically on the positions $\{\vec{R}_i\}$ of the colloidal particles. Ω can be systematically expanded in terms corresponding to the number of colloids:[7,8]

$$\Omega = \sum_{n=0}^{N_c} \Omega_n \tag{6}$$

Ω_0 is the free energy of the pure polymer solution at chemical potential μ_p, in the volume V of interest, Ω_1 is the free energy cost of inserting independent single colloids, Ω_2 takes pairwise colloid−colloid interactions into account, and so forth for higher order terms. Such an expansion can also be carried out near a single wall of area A, where the first few terms are

$$\Omega_0 = -P_p(\mu_p)V + \gamma_{w,p}(\mu_p)A$$

$$\Omega_1 = N_c\omega_1(\mu_p) + \sum_{i=1}^{N_c} \varphi_c^{eff}(z_i)$$

$$\beta\Omega_2 = \sum_{i<j}^{N_c} \beta v_{eff}(R_{ij}) \tag{7}$$

where $\varphi_c^{eff}(z)$ is the effective wall−colloid depletion potential induced by the presence of polymers, $P_p(\mu_p)$ is the osmotic pressure of the bulk polymer solution, and $\gamma_{w,p}(\mu_p)$ is the surface tension induced by the flat wall. Surface tensions are defined throughout relative to the position of the hard wall, at $z = 0$. Inserting a single colloid into a bulk polymer solution costs a free energy $\omega_1(\mu_p) = \Omega_1^{bulk}/N_c$, and $\varphi_c^{eff}(z)$ describes the correction to that insertion free energy when the colloid is at a distance z from the wall. $v_{eff}(R_{ij})$ is the effective interaction between two colloids, induced by the polymer solution. The next higher order contributions to Ω includes a a three-body colloid term, a three-body colloid−colloid−wall term, etc. These will be ignored in the present work.

Brader et al. systematically worked out this expansion for an AO mixture near a flat wall, finding[8] $\beta\Omega_0 = -\rho_p^r(V - R_pA)$ (because $\beta P_p(\mu_p) = \rho_p^r$ and $\beta\gamma_{w,p}^{id} = \rho_p^r R_p$ for AO particles[20]), $\beta\Omega_1 = N_c\rho_p^r(4/3)\pi(R_c + R_p)^3 + \sum_{i=1}^{N_c}\beta\varphi_{AO}(z_i)$, and $\beta\Omega_2 = \sum_{i<j}\beta v_{AO}(R_{ij})$. $\beta\varphi_{AO}(z_i)$ acts on each colloid independently and takes the form

$$\beta\varphi_{AO}(z) = -\frac{\eta_p^r}{4q^3}(2q - z)^2(3 + q + z)\theta(2q - z) \tag{8}$$

where $\eta_p^r = 4\pi\rho_p^r R_p^3/3$ is the polymer packing fraction in the reservoir, $q = R_p/R_c$ is the size ratio, and $\theta(x)$ is the Heaviside step function ($\theta(x) = 0$, $x < 0$; $\theta(x) = 1$, $x > 0$). $v_{AO}(R_{ij})$ is the Asakura−Oosawa depletion[13] potential between two spheres in a bath of ideal polymers; defining now $s = (R - 2R_c)/R_c$, v_{AO} is given by

$$\beta v_{AO}(s) = -\frac{\eta_p^r}{16q^3}(2q - s)^2(6 + 4q + s)\theta(2q - s) \tag{9}$$

The effective Hamiltonian for the AO model, with Ω restricted to the zero-, one-, and two-body terms in eq 6, is strictly valid only for size ratios $q < 0.1547$; for larger size ratios, three- and more-body effective interactions between colloidal particles come into play,[8] but explicit calculations of bulk properties show that they do not play a significant role for q up to ≈ 1.[21,22] Subsequent calculations will neglect more than two-body interactions. For the AO model, Ω_0 and the bulk part of Ω_1, $\Omega_1^{bulk} = N_c\omega_1$, do not affect the interfacial profiles but

do make contributions to the surface tension γ, as will be shown in subsequent sections.

The AO pair potential (eq 9) assumes ideal polymers to be spherical, so that the width of the depletion layer is always equal to $2R_p$. However, polymers can "wrap" around colloidal spheres, the more so the smaller the radius R_c of the latter. Hence, one expects the width of the depletion layer around a colloid to shrink as R_c decreases. This effect can be accounted for by following the prescription of refs 23 and 24, whereby the AO form (eq 9) of the effective pair potential holds, but with a renormalized size ratio q' and a renormalized polymer packing fraction $\eta_p^{r\prime}$:

$$q' = \left(1 + \frac{6}{\sqrt{\pi}}q + 3q^2\right)^{1/3} - 1$$

$$\eta_p^{r\prime} = \left(\frac{q'}{q}\right)^3 \eta_p^r \tag{10}$$

For interacting polymers we can also carry out an expansion of Ω. Accurate expressions for P_p, $\gamma_{w,p}$, ω_1, and $v_{eff}(r)$ are known and have been validated by computer simulations for self-avoiding walk (SAW) chains,[20,24] so that Ω_0, Ω_1, and Ω_2 directly follow from eq 7. The Derjaguin approximation, which is reasonably accurate for an ideal polymer depletant, is expected to remain valid in the case of interacting polymers, at least for sufficiently small q, so that the required wall−colloid effective depletion potential $\varphi_c^{eff}(z_i)$ is given by

$$\beta\varphi_{int}(s) \approx 2\beta v_{int}(s) \tag{11}$$

where the effective potential between two colloids induced by interacting polymers is well approximated by the semiempirical form

$$\beta v_{int}(s) = -\pi \frac{\beta R_c^{\,2} \gamma_{w,p}(\rho_p^r)}{d(\rho_p^r)} [s - d(\rho_p^r)]^2 \theta(d - s) \tag{12}$$

Here $d = D/R_c$ and D is the range of the depletion potential:

$$D(\rho_p^r) = \sqrt{\pi} \frac{\gamma_{w,p}(\rho_p^r)}{P_p(\rho_p^r)} \frac{q'}{q} \tag{13}$$

Because $v_{int}(r)$ depends on polymer density only through ρ_p^r (i.e., μ_p), its form does not change when the polymer density is inhomogeneous. In contrast to the AO model, higher order colloid−colloid and colloid−wall terms are relevant for any size ratio.

The effective one-component representation of colloid−polymer mixtures is thus fully defined, both for ideal and interacting polymers. The next step is to define the density functional appropriate for the description of the inhomogeneous effective one-component model.

III. Density Functional Formulation

Given the effective Hamiltonian specified by eqs 5 and 7, one may construct an approximate free energy density functional to investigate the properties of the inhomogeneous effective one-component system of colloidal particles. The latter interact via a hard sphere repulsions (for $r < 2R_c$) and a polymer-induced depletion attraction that will be described within first-order perturbation theory,[25] which is expected to be accurate for not too small values of q (i.e., for sufficiently long-range attractions). The intrinsic free-energy functional is then conveniently split into ideal, hard sphere, and perturbation parts; for the hard core part we adopt the very accurate "White Bear" version[26] of Rosenfeld's "fundamental measure" (FMT) functional[17]

$$F[\rho_c(\vec{r})] = F_{id}[\rho_c(\vec{r})] + F_{FMT}[\rho_c(\vec{r})] + F_1[\rho_c(\vec{r})] \tag{14}$$

The ideal contribution is

$$F_{id}[\rho_c] = k_B T \int d\vec{r}\ \rho_c(\vec{r})[\ln(\Lambda_c^{\,3}\rho_c(\vec{r})) - 1] \tag{15}$$

where Λ_c is an irrelevant colloidal length scale. The FMT-hard core contribution is of the "weighted density" type, namely

$$\beta F_{FMT}[\rho_c] = \int d\vec{r}\ [\Phi_1(\{n_j(\vec{r})\}) + \Phi_2(\{n_j(\vec{r})\}) + \Phi_3(\{n_j(\vec{r})\})] \tag{16}$$

where the $n_j(\vec{r})$ are weighted densities of the form

$$n_j(\vec{r}) = \int \omega^{(j)}(\vec{r} - \vec{r}')\, \rho_c(\vec{r}')\, d\vec{r}' \tag{17}$$

The functions Φ_i and the weight functions $\omega^{(j)}(\vec{r})$ are defined in Appendix A. Finally, the first-order perturbation term reads

$$F_1[\rho_c] = \int d\vec{r}\ \rho_c(\vec{r})\, \Psi_1(\vec{r}) \tag{18}$$

with

$$\Psi_1(\vec{r}) = \frac{1}{2} \int d\vec{r}'\, \rho_c(\vec{r}')\, v(|r - r'|)\, g_{hs}(|r - r'|, \bar{\rho}_c(\vec{r}, \vec{r}')) \tag{19}$$

where $v(r) = v_{AO}(r)$ or $v_{int}(r)$ is the depletion potential induced by ideal (AO) or interacting (int) polymer coils; g_{hs} is the pair distribution function of the homogeneous reference hard sphere fluid, evaluated at an intermediate density between the two points $\vec{r}$ and $\vec{r}'$:

$$\bar{\rho}_c = \frac{\bar{\rho}_\nu(\vec{r}) + \bar{\rho}_\nu(\vec{r}')}{2} \tag{20}$$

with

$$\bar{\rho}_\nu(\vec{r}) = \frac{3}{4\pi R_\nu^{\,3}} \int_{|r - r'| < R_\nu} \rho_c(\vec{r}')\, d\vec{r}' \tag{21}$$

$\bar{\rho}_\nu(\vec{r})$ is a smoothed density profile around $\vec{r}$; the radius R_ν is of the order of R_c, and results are not expected to be very sensitive to the precise value of R_ν. Following the earlier experience of ref 27 we have chosen $R_\nu = 1.6R_c$. The form (19) is the generalization of the standard first order thermodynamic theory[32] to inhomogeneous fluids. The choices given in eq 20 and 21 have proved very adequate in many DFT calculations of fluids near hard walls.

In the homogeneous limit, where the density profile reduces to the bulk density, the free energy given by eq 14 goes over to the Helmholtz free energy of the fluid phase calculated within first-order thermodynamic perturbation theory,[28] which leads to reasonable phase diagrams of colloid−polymer mixtures.[22] The familiar generalized van der Waals mean field approximation amounts to setting $g_{HS}(r) = \theta(2R_c - r)$, which leads of course to a considerable simplification of the DFT calculations.

Keeping in mind that the total effective Hamiltonian of the colloids is given by eqs 5−7, with $\Omega = \Omega_0 + \Omega_1 + \Omega_2$, the grand potential functional to be minimized with respect to the

density profile $\rho_c(\vec{r})$ is the sum of the intrinsic free energy functional 14 and of the contributions from the external fields:

$$\Omega_\varphi[\rho_c] = F[\rho_c] + \int \rho_c(\vec{r})[\varphi_c(\vec{r}) - \mu_c^0]\, d\vec{r} + \Omega_0 + \Omega_1^{bulk} \quad (22)$$

where μ_c^0 is the bulk chemical potential of the colloids, whereas Ω_0 and $\Omega_1^{bulk} = N_c\omega_1$ are defined in eq 7. Because the latter are constants, they have no influence on the equilibrium profile $\rho_c(\vec{r})$, but they will contribute to the equilibrium value of the grand potential, and hence to the surface tension. $\varphi_c(\vec{r}) = \varphi_c^0(\vec{r}) + \varphi_c^{eff}(\vec{r})$ is the sum of the external potential acting directly on the colloidal particles ($\varphi_c^0(\vec{r})$) and of the polymer-induced depletion contribution, $\varphi_c^{eff}(\vec{r})$, given by eq 8 or 11 for ideal and interacting polymers, respectively.

The Euler−Lagrange equation of the variational problem reads

$$\frac{\delta\Omega_\varphi[\rho_c(\vec{r})]}{\delta\rho_c(\vec{r})} = \frac{\delta F[\rho_c(\vec{r})]}{\delta\rho_c(\vec{r})} + \varphi_c(\vec{r}) - \mu_c^0 = 0 \quad (23)$$

F is the sum of ideal (F_{id}) and excess ($F_{ex} = F_{FMT} + F_1$) parts; defining the local excess chemical potential as

$$\mu_c^{ex}(\vec{r}) = \frac{\delta F_{ex}[\rho_c(\vec{r})]}{\delta\rho_c(\vec{r})} = \frac{\delta F_{FMT}[\rho_c(\vec{r})]}{\delta\rho_c(\vec{r})} + \frac{\delta F_1[\rho_c(\vec{r})]}{\delta\rho_c(\vec{r})} \quad (24)$$

the Euler−Lagrange equation may be cast in the form

$$k_BT \ln[\Lambda_c^3\rho_c(\vec{r})] + \mu_c^{ex}(\vec{r}) = \mu_c^0 - \varphi_c(\vec{r}) \quad (25)$$

so that the density profile satisfies the nonlinear equation:

$$\rho_c(\vec{r}) = \rho_c^0 \exp\{-\beta[\varphi_c(\vec{r}) + \mu_c^{ex}(\vec{r}) - \mu_c^{0,ex}]\} \quad (26)$$

where $\mu_c^{0,ex}$ is the excess part of the bulk chemical potential of the colloids. The coupled equations (24) (with F_{FMT} and F_1 given by eqs 16 and 18) and (26) must be solved numerically by standard iterative procedures.

Because only planar interfaces will be considered, the external potential, the density profile, and local chemical potential all depend only on z, the coordinate orthogonal to the plane of the interface. The corresponding simplified expression for the local excess chemical potential $\mu_c^{ex}(\vec{r})$[29] is given in Appendix B, together with the weight functions $\omega^{(j)}(z-z')$ appropriate for the one-dimensional problem.

Once the equilibrium profile $\rho_c(z)$ has been determined, it can be substituted into the expression of the functional 22 to determine the equilibrium grand potential Ω. Subtraction of the bulk contribution then allows the surface tension γ to be calculated, according to the definition:

$$\gamma = \frac{\Omega + PV}{A} \quad (27)$$

where P is the total bulk osmotic pressure of the mixture and A the total area of the planar interface.

IV. Density Profiles near a Hard Wall

Consider first the case of a colloid−polymer mixture near a hard wall placed at $z = 0$. The density profiles were calculated by solving the one-dimensional versions of eqs 24 and 26 (see Appendix B). A systematic comparison is made between profiles for ideal and interacting polymers, over a range of colloid and polymer packing fractions η_c^0 and η_p^r and for size ratios ranging from $q = 0.34$ to $q = 1.05$. Parts a and b of Figure 1 compare the density profiles calculated for a fixed colloidal density and several polymer concentrations, for interacting and ideal polymers. As expected, the colloid adsorption at contact increases dramatically with increasing polymer concentration, due to the enhanced effective depletion-induced attraction to the wall. The effect is stronger for ideal polymers, which also lead to strong layering at the highest packing fraction, hinting at a possible layering transition. The enhanced adsorption and layering are easily understood, because the polymer induced attraction is substantially stronger for ideal polymers (cf. eq 8) compared to interacting polymers (eqs 12 and 11), at the same R_p, q, and ρ_p^r.[20] The structured profile at $\eta_p^r = 0.4$ in Figure 1b is for a thermodynamic state close to the fluid−fluid binodal (on the colloid-poor "vapor side") calculated from the same free energy model (see ref 22) giving further support to the possibility of a layering transition.[30,31]

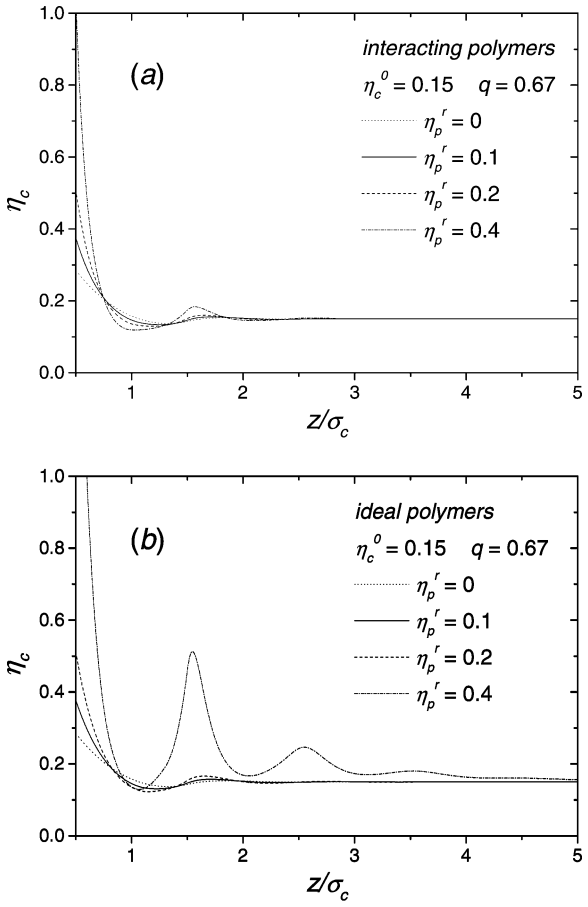

Figure 1. Colloid density as a function of the distance to the hard wall for mixtures of colloids and (a) interacting polymers and (b) ideal polymers, at different polymer concentrations. In both figures the bulk colloid packing fraction and the size ratio were set at $\eta_c^0 = 0.15$ and $q = 0.67$.

The effect of the range of the depletion attraction is illustrated in Figure 2a,b for interacting and ideal polymers, respectively. The trend of the density profiles with increasing q is opposite that observed with increasing η_p^r. The adsorption at contact is now strongest for the smallest size ratio. This is essentially due to the fact that the wall−colloid depletion potential at contact, $\varphi_c^{eff}(0)$, drops as the polymer density decreases. Because $\rho_p^r \sim \eta_p^r/q^3$, a small increase in the size ratio q implies a big reduction in polymer density, and also in $\varphi_c^{eff}(0)$. Calculations carried out at higher colloid packing fractions show that the

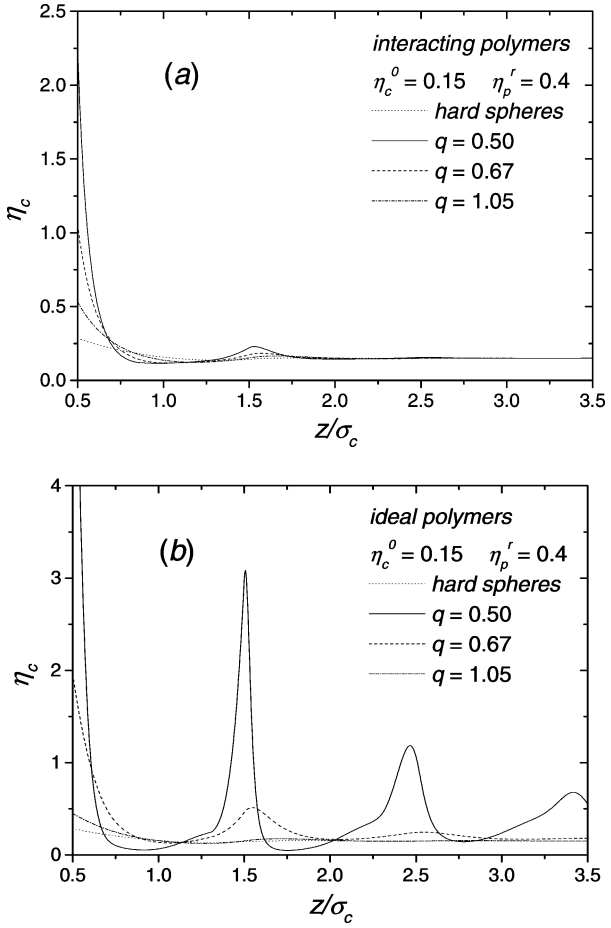

Figure 2. Effect of the polymer−colloid size ratio, q, on the density profile near a hard wall for $\eta_c^0 = 0.15$ and $\eta_p^r = 0.4$ induced by (a) interacting and (b) ideal polymers. In both figures, the density profile of pure one-component hard spheres (without depletant) at $\eta_c^0 = 0.15$ has been included for comparison.

effect of polymer-induced wall−colloid attraction on the density profiles is much reduced as η_c^0 increases, due to the predominance of purely excluded volume effects under high-density conditions.[28,32]

V. Wall Surface Tension

Once the colloid density profiles have been calculated, the surface tension may be determined by substituting $\rho_c(z)$ into eq 22, and then applying relation 27. Some care has to be taken in treating the bulk zero and one-body contribution Ω_0 and Ω_1^{bulk}. These also contribute to the bulk properties (calculated by letting $\rho_c(z)$ go to the bulk value ρ_c^0), and in particular to the colloid chemical potential μ_c^0 and to the osmotic pressure of the mixture. Thus, for the chemical potential of the bulk one obtains

$$\mu_c^0 = \mu_c(\rho_c^0) + \omega_1 \tag{28}$$

where ω_1 is already defined in eq 7.

In a similar fashion, the total osmotic pressure is the sum of the colloid contribution $P_c(\rho_c^0,\rho_p^r)$ (calculated by differentiating the homogeneous limit of the intrinsic free energy (14) with respect to ρ_c^0) and of the osmotic pressure of the polymer reservoir:

$$P = P_c(\rho_c,\rho_p^r) + P_p(\rho_p^r) \tag{29}$$

Hence,

$$\frac{\Omega + PV}{A} = \frac{\Omega_0 + \Omega_1 + \Omega_2 + PV}{A} = \left\{\frac{-P_p V + \gamma_{w,p} A}{A}\right\} + \{\omega_1(\rho_p^r)\int dz\, \rho_c(z) + \int dz\, \rho_c(z)\, \varphi_c(z)\} + \left\{\frac{F[\rho_c(z)]}{A} - \mu_c^0 \int dz\, \rho_c(z)\right\} + \frac{PV}{A} \tag{30}$$

where $F[\rho_c(z)]$ is the colloid contribution to the inhomogeneous free energy, given by eq 14. Substituting eqs 28 and 29 shows that the bulk contributions to Ω_0 and Ω_1 are exactly canceled so that the final expression for the surface tension is given by

$$\gamma_w = \lim_{L\to\infty} \frac{\Omega + PV}{A} = \gamma_{w,p} + \lim_{L\to\infty} \int_0^L dz\, \{f[\rho_c(z)] + \rho_c(z)[\varphi_c(z) - \mu_c(\rho_c^0)] + P_c\} \tag{31}$$

where $f = F/V$ is the intrinsic colloid free energy density (14). In other words, the surface tension may be written as the sum of a colloid contribution $\gamma_{w,c}$ (which would be obtained by ignoring Ω_0 and Ω_1^{bulk} in eq 22) and of the contribution of the polymers under reservoir conditions:

$$\gamma_w = \gamma_{w,c}(\rho_c^0,\rho_p^r) + \gamma_{w,p}(\rho_p^r) \tag{32}$$

Equation 32 is exact within an effective one-component representation of a mixture of colloids and polymers where Ω in eq 6 is truncated at Ω_2. For the $\gamma_{w,c}(\rho_c^0,\rho_p^r)$ of interacting (SAW) polymers, we use the results of ref 24. The resulting total surface tensions for the cases of ideal and interacting polymers are plotted as a function of the polymer reservoir packing fraction in Figure 3 and compared to the predictions of the two-component representation (with ideal polymers), calculated within scaled particle theory,[10] modified so as to account for the "polymer wrapping" effect, according to the prescriptions of eq 10.

The agreement between the surface tensions calculated within the effective one- and two-component representations is seen to be good for low densities and to deteriorate somewhat beyond. The surface tension with interacting polymers is substantially larger (up to a factor of 2 at the highest polymer concentrations) compared to the ideal polymer case. This is because the colloid−wall surface tension is higher with interacting polymers, due to the weaker effective wall−colloid attraction, and the wall−polymer surface tension is also higher for interacting polymers.[20]

Figure 4 illustrates the variation of the surface tension with size ratio q. For fixed values of η_c^0 and η_p^r, the surface tension is seen to decrease rapidly as q increases, and to tend to the result for hard spheres when $q > 1$. Finally, the variation of the surface tension with colloid packing fraction (for fixed q and η_p^r) is shown in Figure 5. The agreement between the effective one and two-component representations found at low packing fractions is seen to deteriorate rapidly as η_c^0 increases, thus illustrating the break-down of the effective one-component model for highly concentrated colloidal suspensions.

VI. Depletion Interaction between Hard Walls

The depletion potential per unit area induced by a colloid−polymer mixture between two hard walls of area A separated by L is determined by

$$W(L) = \frac{\Omega(L) - \Omega(\infty)}{A} \tag{33}$$

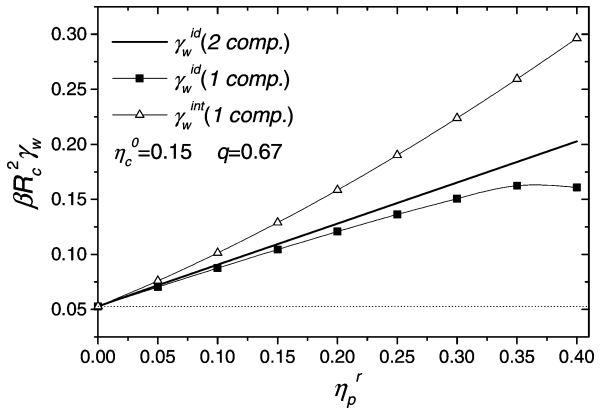

Figure 3. Wall surface tension for ideal (squares) and interacting polymers (triangles) in the one-component representation, and for ideal polymers in the two-component representation (solid line), as a function of η_p^r ($\eta_c^0 = 0.15$ and $q = 0.67$). The dotted horizontal line is for hard sphere colloids only (without depletant).

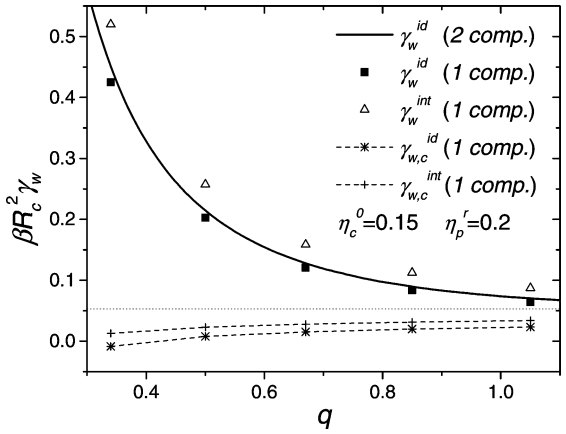

Figure 4. Wall surface tension for ideal (squares) and interacting (triangles) polymers in the one-component representation, and for ideal polymers in the two-component representation (solid line), as a function of the size ratio, q ($\eta_c^0 = 0.2$ and $\eta_p^r = 0.2$). The dotted horizontal line is for pure hard spheres, and the colloidal contributions to the wall surface tension, $\gamma_{w,c}$, are also shown for comparison.

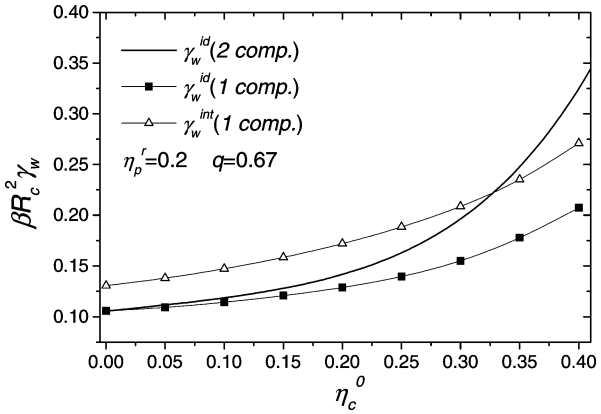

Figure 5. Wall surface tension for ideal (squares) and interacting (triangles) polymers in the one-component representation, and for ideal polymers in the two-component representation (solid line), as a function of the bulk colloid packing fraction, η_c^0 ($\eta_p^r = 0.2$ and $q = 0.67$).

Clearly, $W(L) \to 0$ as $L \to \infty$, whereas $W(L=0) = -2\gamma_w$, because when the walls come into contact, two fluid−wall interfaces are destroyed. For arbitrary L, the colloid contribution W_c to $W(L)$ obtained by momentarily ignoring the bulk contributions

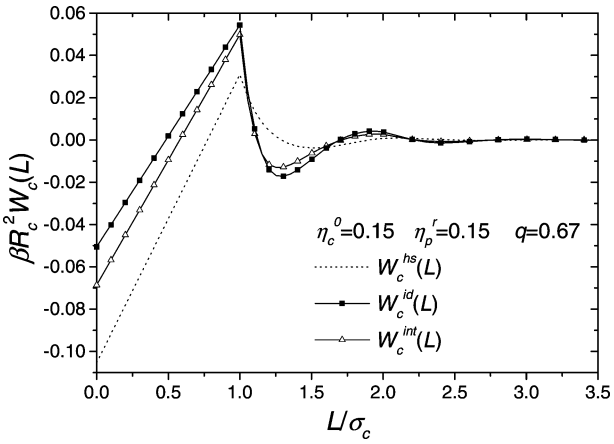

Figure 6. Effective depletion potential between two flat parallel walls as a function of the wall−wall distance, L, induced by pure hard colloids (dotted line), colloids plus ideal polymers (triangles), and colloids plus ideal polymers (squares). $\eta_c^0 = 0.15$, $\eta_p^r = 0.15$, and $q = 0.67$.

Ω_0 and Ω_1^{bulk} to the total grand potential, reads, by straightforward analogy with expression (31) for the surface tension:

$$W_c(L) = \int_0^L dz \{F[\rho_c(z)] + \rho_c(z)[\varphi_c(z) - \mu_c(\rho_c^0)] + P_c\} - 2\gamma_{w,c} \quad (34)$$

Figure 6 shows the comparison of the depletion potentials $W_c(L)$ calculated for a pure hard sphere depletant (i.e., $\eta_p^r = 0$) and for hard sphere colloids and ideal or interacting polymers, within the present effective one-component representation. The extra attraction between the walls and colloidal particles forces the latter into the region between the two plates, enhancing the potential barrier of the depletion potential at $L = R_c$. The effect is stronger for ideal than for interacting polymers, because effective wall−colloid and colloid−colloid attractive interactions are enhanced in going from interacting to ideal polymers. For $L < 2R_c$ the hard colloids are excluded from the space between the walls, and the depletion potential is entirely controlled by the external, unbalanced osmotic pressure which pushes the walls together, i.e.:

$$W_c(L<2R_c) = P_c L - 2\gamma_{w,c} \quad (35)$$

To obtain the total depletion potential, the volume terms Ω_0 and Ω_1^{bulk} must be included in the grand potential. It is easily verified that, within the truncation of Ω at Ω_2, i.e., ignoring colloid−colloid−polymer and similar higher order terms, the depletion potential takes the form

$$W(L) = \begin{cases} W_c(L) + P_p^r L - 2\gamma_{w,p}(\rho_p^r) & L < D_w^p \\ W_c(L) & L \geq D_w^p \end{cases} \quad (36)$$

where P_p^r is the osmotic pressure of the polymers in the reservoir, $\gamma_{w,p}$ is the corresponding wall−polymer surface tension, and $D_w^p = 2\gamma_{w,p}/P_p$ is the range of the polymer depletion potential, which takes the value $D_w^{id} = 2R_p$ for AO particles. The resulting total depletion potential for ideal polymers is shown in Figure 7. It remains continuous at $L = 2R_p$, but the resulting force is discontinuous at that separation.

The basic input in the evaluation of surface tensions or depletion forces are the density profiles $\rho_c(z)$. To check the reliability of the profiles calculated within the present perturbation DFT, we have carried out some grand canonical Monte Carlo (GCMC) simulations of profiles, using the same effective

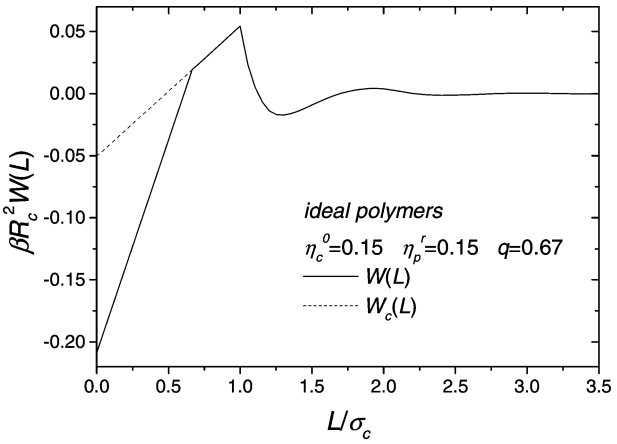

Figure 7. Comparison between the wall−wall depletion potential in a mixture of colloids and ideal polymers, with and without the bulk contributions to the free energy (W and W_c, respectively). $\eta_c^0 = 0.15$, $\eta_p^r = 0.15$ and $q = 0.67$.

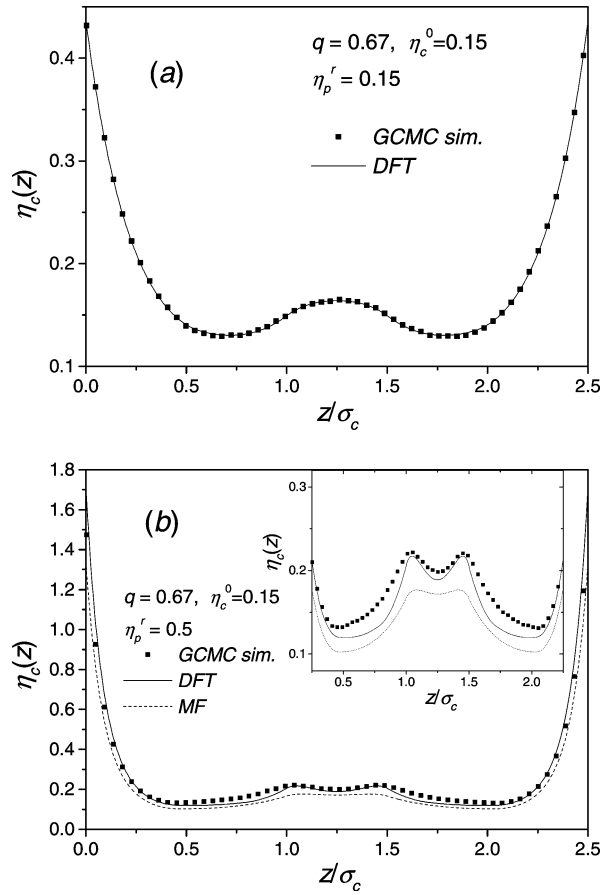

Figure 8. (a) Colloid packing fraction between two hard walls obtained using GCMC simulations (squares) and DFT (solid line) for a mixture of colloids and interacting polymers and for $q = 0.67$, $\eta_c^0 = 0.15$, and $\eta_p^r = 0.15$. (b) Same as Figure 8a, but with $\eta_p^r = 0.5$. Dashed lines are the results obtained from the mean-field DFT theory (MF). The inset shows a magnification of the inner part of the data for better comparison.

colloid−colloid and colloid−wall interactions as with DFT. Two typical examples of such a comparison are shown in Figure 8a,b for a mixture of colloids and interacting polymers confined between two hard walls (slit geometry). At the lower polymer concentrations, corresponding to relatively weak colloid−colloid and wall−colloid attraction, the agreement between DFT and simulation is excellent (Figure 8a). At the higher polymer concentration (Figure 8b), the attractive perturbation is much stronger and, as expected, the agreement worsens. Nevertheless, the perturbation DFT is still capable of reproducing the main features of the density profile. Figure 8b also shows the result from the mean-field DFT, which amounts to neglecting correlations in $F_1[\rho_c]$ (cf. section III). The disagreement with the simulated data is now much more severe (see the inset in Figure 8b), stressing the importance of properly including reference system correlations in eq 19.

VII. Fluid−Fluid Interface

We finally turn to the fluid−fluid interface at coexistence between colloid-poor ("gas") and colloid-rich ("liquid") phases. This is a "free" interface, because translational symmetry is broken in the absence of any external potential, i.e., $\varphi_c(\vec{r}) = 0$. An accurate and consistent determination of the phase boundary (binodal) in the η_c^0 (colloid packing fraction)−η_p^r (polymer reservoir packing fraction) is required. The bulk free energy per unit volume, obtained from eqs 14−19 in the homogeneous ($\rho_c(\vec{r}) = \rho_c^0$) limit, reads

$$\beta f = \rho_c^0\left[\ln(\rho_c^0) - 1 + \frac{\eta_c^0(4 - 3\eta_c^0)}{(1 - \eta_c^0)^2}\right] + \frac{(\rho_c^0)^2}{2}\int \mathrm{d}\vec{r}\; g_{HS}(r,\rho_c^0)\,\beta v(r) \quad (37)$$

This free energy depends implicitly on the polymer concentration η_p^r via the effective depletion pair potential $v(r) = v(r;\eta_p^r)$, which is given by eq 9 (v_{AO}) for ideal polymers and by eq 12 (v_{int}) for interacting polymers.

For any fixed value of η_p^r the colloid packing fractions of the coexisting phases may be determined by applying the standard Maxwell double-tangent construction to f. The resulting binodals for ideal and interacting polymers (not shown) are very close to those calculated in ref 22, where an estimate of the second-order perturbation correction to the free energy was included. The trends of the binodals are according to expectation. Qualitatively, the behavior for ideal and interacting polymers is similar, with critical points at higher η_p^r as q increases, but with considerably "flatter" binodals for interacting polymers. There are, however, very significant quantitative differences, because the binodals for interacting polymers are shifted to considerably larger values of η_p^r for each size ratio q, i.e., polymer interactions enhance the miscibility of colloid−polymer mixtures. This is easily understood, because the polymer-induced depletion attraction between colloids is weaker (for given q and η_p^r) for interacting polymers.

The colloid density profile at the fluid−fluid interface is calculated by minimizing the grand potential (eq 22), with $\varphi_c \equiv 0$, which leads back to expression 26 (again with $\varphi_c \equiv 0$). The profiles for ideal and interacting polymers are shown in Figures 9 and 10, under conditions close to the fluid−fluid−solid triple point, for a size ratio $q = 0.67$. The profiles are compared to earlier predictions based on a square gradient density functional (SGT),[12] using the same effective one-component description. There are remarkable differences between the profiles corresponding to interacting and ideal polymers. The interface is much sharper in the latter case and exhibits striking oscillations on the high colloid density ("liquid") side.[9] The profile obtained with interacting polymers varies more smoothly and shows no sign of oscillations. This clear-cut difference in behavior may be partly understood by noting that the jump in colloid density between the two fluid

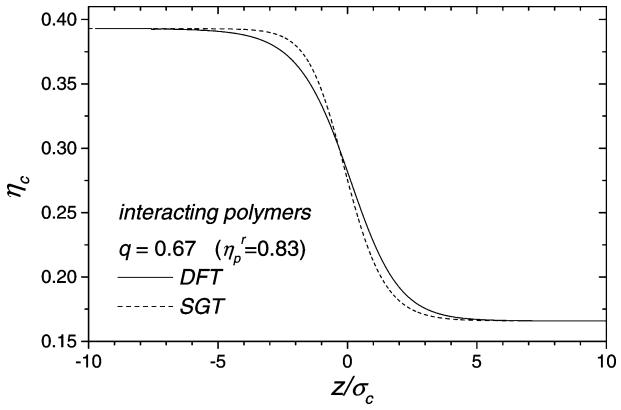

Figure 9. Comparison between the colloid density profile for *interacting* polymers obtained using our perturbative DFT (solid line) and the square gradient approximation SGT (dashed line), for $\eta_p^r = 0.83$ and $q = 0.67$ (close to the triple point).

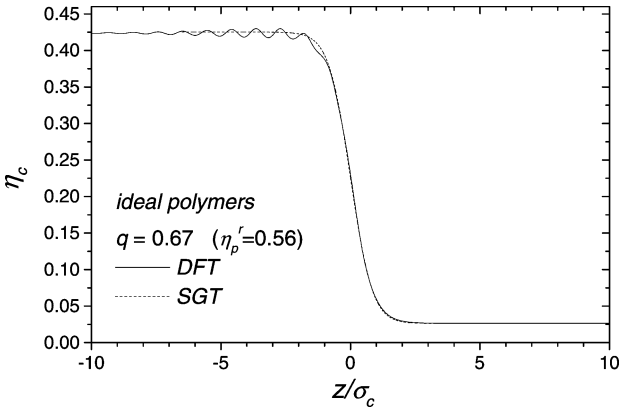

Figure 10. Comparison between the colloid density profile for *ideal* polymers obtained using our perturbative DFT (solid line) and the square gradient approximation SGT (dashed line), for $\eta_p^r = 0.56$ and $q = 0.67$ (close to the triple point).

phases is significantly smaller in the case of interacting polymers, for which the triple and critical points are much closer than for ideal polymers. Figures 9 and 10 also show the result of our earlier square gradient calculations (SGT).[12] The corresponding profiles agree reasonably well with the results of the more elaborate density functional used in this paper; as expected, the square gradient functional cannot account for the oscillatory structuring on the dense fluid side in Figure 10.

In the case of interacting polymers (Figure 9) the width of the interface predicted by the present perturbation DFT is significantly larger than that obtained from square gradient theory. The interfacial width *w* is conventionally defined as the distance between the two points where the density profile $\rho_c(z)$ reaches 90% and 10% of the difference between the bulk densities of the two coexisting phases. Results for *w* obtained within the perturbation DFT are plotted in Figure 11 as a function of the deviation of the polymer reservoir packing fraction from its value at the critical point, $\alpha = (\eta_p^r - \eta_p^{r,crit})/\eta_p^{r,crit}$, for ideal and interacting polymers and for three size ratios *q*. As expected, the width increases with *q* and increases sharply as α decreases, i.e., upon approaching the critical point. Although the widths *w* for ideal and interacting polymers are rather close for given α and *q*, polymer interactions tend to reduce the width compared to the ideal case, as found in ref 12.

The surface tension γ of the fluid−fluid interface is given by a relation similar to eq 31, and it is easily verified that the

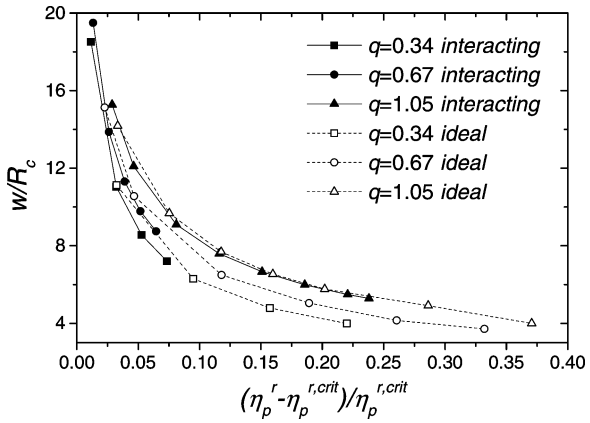

Figure 11. Interfacial width obtained using the perturbation DFT for interacting polymers (solid lines and black symbols) and ideal polymers (dashed lines and white symbols), and for $q = 0.34$, 0.67, and 1.05.

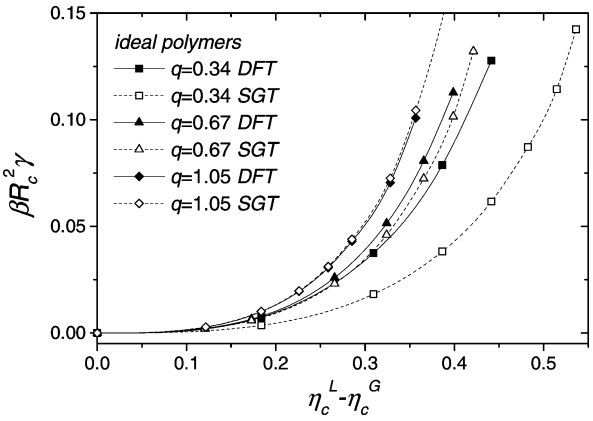

Figure 12. Comparison between the surface tension of the gas−liquid interface obtained from our perturbation DFT (solid lines and black symbols) and the square gradient theory SGT (dashed lines and white symbols), for ideal polymers.

bulk terms Ω_0 and Ω_1^{bulk} in eq 22 do not contribute to γ. The relation reads

$$\gamma = \int_{-\infty}^{\infty} dz \, \{f[\rho_c(z)] - \rho_c(z)\mu_c^0 + P_c\} \qquad (38)$$

where μ_c^0 and P_c are the common values of the colloid contribution to the chemical potential and of the pressure in the coexisting bulk phases. Figure 12 compares results obtained from the perturbation and square gradient theories for ideal polymers, at three different size ratios; γ is plotted versus the difference between the colloid packing fractions in the "liquid" and "gas" phases. The surface tensions are seen to increase with *q* and $\eta_c^L - \eta_c^G$. The agreement between the two theories is excellent for $q = 1.05$ and deteriorates for smaller size ratios. The surface tensions obtained from perturbation DFT are systematically larger than their square gradient counterparts and closer to the results of the two-component DFT of ref 9.

A comparison between the surface tensions calculated within perturbation DFT for ideal and interacting polymers is finally made in Figure 13. The surface tension is seen to be lowered when polymer interactions are included, a trend that is opposite to that observed for the wall surface tension γ_w (cf. Figure 4).

A fluid−fluid interface also implies an inhomogeneous polymer density profile. For ideal polymers at constant μ_p this does not cost any additional free energy, but this is not true for interacting polymers. For the latter depletant, this correction will raise the surface tension compared to the values we calculate

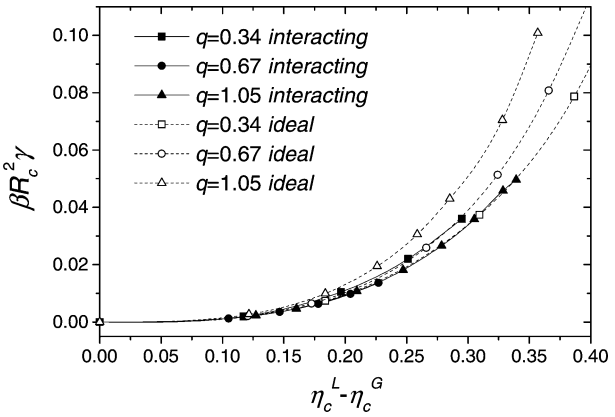

Figure 13. Surface tension of the free liquid−gas interface for interacting polymers (solid lines and black symbols) and ideal polymers (dashed lines and white symbols), and for $q = 0.34$, 0.67, and 1.05.

within the one-component picture. On the other hand, for ideal polymers, the many-body interactions between the colloids, fully taken into account with the two-component formulation, also result in a larger surface tension. The effect of many-body interactions for interacting polymers is unknown. Thus our prediction for the relative strength of the surface tensions should be tempered by the fact that the exact form of the neglected corrections is not known and awaits a full two-component treatment of interacting polymer−colloid mixtures.

VIII. Conclusion

We have introduced a simple generic density functional description of colloid−polymer mixtures within the effective one-component picture where polymer degrees of freedom have been traced out. The free energy functional accounts correctly for the colloid excluded volume effects and treats the polymer-induced depletion attraction within first order perturbation theory. The DFT formulation is very flexible and can be applied to confined colloid−polymer mixtures as well as to the free interface between coexisting fluid phases. Although this effective one-component description accounts only for pairwise additive depletion interactions and neglects more-than-two-body effective interactions (which are automatically included in an effective two-component representation), the present theory has the advantage of being able to treat the cases of ideal as well as interacting polymers consistently, thus allowing a direct estimate of the effect of polymer interactions on the interfacial properties of colloid−polymer mixtures. The present effective one-component DFT description can be tested against the more fundamental two-component DFT picture in the case of ideal polymers.[9,10] Reasonable agreement is found for size ratios up to $q \approx 1$, giving confidence in the predictions of the simpler one-component representation for ideal and interacting polymers alike. The reduction to an effective one-component representation leads to the appearance of zero- and one-body bulk contributions to the total grand potential of the mixture (terms Ω_0 and Ω_1^{bulk} in eq 22), which make significant contributions to the wall surface tension γ_w and to the depletion interaction between two walls and must not be overlooked. The key findings of the present investigation may be summarized as follows:

•Density profiles $\rho_c(z)$ near a hard wall deviate considerably from pure hard sphere behavior at low colloid packing fractions. Significant differences between the behavior observed for ideal and interacting polymers may be traced back to the weaker depletion attraction induced by the latter.

•When the bulk terms Ω_0 and Ω_1^{bulk} in the grand potential are properly taken into account, the wall surface tensions γ_w calculated with ideal polymers are in good agreement with a recent full two-component treatment of the AO model,[10] for $q \leq 1$ and not too high colloid packing fraction η_c.

•The depletion potential induced by colloid−polymer mixtures between two walls exhibits structure on both length scales R_c and R_p, which opens the possibility of further flexibility in "engineering" effective depletion forces.

•In general, the wall surface tension γ_w induced by mixtures of colloids and interacting polymers is larger than that found for ideal polymers. This trend is opposite to that predicted for the fluid−fluid interfacial tension. The present predictions agree at least qualitatively with the experimental data of ref 4.

•The present effective one-component DFT predicts an oscillatory density profile on the high colloid density side of the fluid−fluid interface in the case of ideal polymers sufficiently close to the triple point; this behavior agrees with the earlier prediction based on the effective two-component (AO model) representation.[9] The oscillations are not observed in the case of interacting polymers, presumably due to the smoother variation (larger width) of the interfacial profile near the triple point.

•A direct comparison between the results of square gradient analysis[12] and the present more sophisticated DFT shows that the former is surprisingly accurate, even for rather sharp fluid−fluid interfaces (except, of course, as regards the oscillatory behavior observed for ideal polymers). The good agreement validates the predictions of the simple square gradient theory concerning the effect of polymer−polymer interactions on the fluid−fluid interfacial properties.[12]

The present effective one-component description predicts a number of significant differences between interfacial behavior of mixtures of colloids and ideal versus interacting polymer coils. The corresponding two-component representation involving ideal polymers (i.e., the AO model) is well established and confirms many of the predictions of the present effective one-component picture. Future work should focus on developing a viable effective two-component representation in the case of interacting polymers, to validate the present predictions based on the effective one-component description.

Acknowledgment. A.M.-J. thanks the Ministerio de Ciencia y Tecnologıa [Plan Nacional de Investigación Cientıfica, Desarrollo e Innovación Tecnológica (I+D+I), project MAT 2003-08356-C04-01], J.D. acknowledges the EPSRC within the Portfolio grant RG37352, and A.A.L. thanks the Royal Society (London), for financial support. Part of this work was carried out while J.P.H. was on leave at Università degli studi di Roma "La Sapienza", and support of INFM is gratefully acknowledged.

IX. Appendix

A. Fundamental Measure Theory for Hard Spheres. To model the hard sphere nature of the colloidal particles, we have used the White-Bear version of the Rosenfeld functional.[26] This functional improves the one proposed by Rosenfeld[17] in that it

leads to the Mansoori et al. equation of state for a homogeneous mixture.[32] The free energy density $\Phi_{FMT} = \Phi_1 + \Phi_2 + \Phi_3$ reads[26]

$$\Phi_1 = -n_0 \ln(1 - n_3)$$

$$\Phi_2 = \frac{n_1 n_2 - \vec{n}_{V1} \cdot \vec{n}_{V2}}{1 - n_3}$$

$$\Phi_3 = (n_2^3 - 3 n_2 \vec{n}_{V2}^2) \frac{n_3 - (1 - n_3)^2 \ln(1 - n_3)}{36\pi n_3^2 (1 - n_3)^2} \quad (39)$$

where $\{n_j(\vec{r})\}$ are weighted densities, obtained as convolutions of the colloid density $\rho_c(\vec{r})$ and the weight functions $\omega^{(j)}$ (see eq 17). The latter are given by

$$\omega^{(3)}(r) = \theta(R_c - r)$$

$$\omega^{(2)}(r) = \delta(R_c - r)$$

$$\omega^{(V2)}(\vec{r}) = (\vec{r}/r)\delta(R_c - r)$$

$$\omega^{(0)}(r) = \frac{\omega^{(2)}(r)}{4\pi R_c^2} \qquad \omega^{(1)}(r) = \frac{\omega^{(2)}(r)}{4\pi R_c}$$

$$\omega^{(V1)}(\vec{r}) = \frac{\omega^{(V2)}(\vec{r})}{4\pi R_c} \quad (40)$$

B. Particular Case: Planar Geometry. For the case of planar fluid−fluid interfaces or infinite planar walls, the calculations simplify to a one-dimensional problem. Then, the position-dependent excess chemical potential $\mu_c^{ex}(\vec{r})$, which can be obtained from the functional derivative of the excess part of our perturbation free energy functional (eq 24), depends only on z, the distance to the wall (or to the interface). Its explicit form for $z = z_1$ is[29]

$$\beta\mu_c^{ex}(z_1) = \int \sum_j \frac{\partial \Phi_{FMT}[n_j(z_2)]}{\partial n_j(z_2)} \frac{\delta n_j(z_2)}{\delta \rho_c(z_1)} dz_2 +$$
$$2\pi \int_{z_1 - r_m}^{z_1 + r_m} dz_2\, \rho_c(z_2) \int_{|z_1 - z_2|}^{r_m} dr_{12}\, r_{12} \beta v(r_{12})\, g_{hs}(r_{12}, \bar{\rho}_c(z_1, z_2)) +$$
$$\frac{3\pi}{4R_\nu^3} \int_{z_1 - r_m}^{z_1 + r_m} dz_2\, \rho_c(z_2)[R_\nu^2 - (z_1 - z_2)^2] \times$$
$$\int_{z_2 - r_m}^{z_2 + r_m} dz_3\, \rho_c(z_3) \int_{|z_2 - z_3|}^{r_m} dr_{23}\, r_{23} \beta v(r_{23}) \frac{\partial g_{hs}(r_{23}, \bar{\rho}_c(z_2, z_3))}{\bar{\rho}_c} \quad (41)$$

where $v(r)$ is the corresponding colloid−colloid depletion potential, r_m its range and

$$\frac{\delta n_j(z')}{\delta \rho_c(z)} = \omega^{(j)}(z' - z) \quad (42)$$

For planar geometry, the weight functions are given by

$$\omega^{(0)}(z' - z) = \frac{1}{2R_c}\theta(R_c - |z - z'|)$$

$$\omega^{(1)}(z' - z) = \frac{1}{2}\theta(R_c - |z - z'|)$$

$$\omega^{(2)}(z' - z) = 2\pi R_c \theta(R_c - |z - z'|)$$

$$\omega^{(3)}(z' - z) = \pi[R_c^2 - (z - z')^2]\theta(R_c - |z - z'|)$$

$$\vec{\omega}^{(V1)}(z' - z) = \frac{1}{2R_c}(z - z')\theta(R_c - |z - z'|)\vec{k}$$

$$\vec{\omega}^{(V2)}(z' - z) = 2\pi(z - z')\theta(R_c - |z - z'|)\vec{k}$$

where $\vec{k}$ is the unit vector along the z-axis. The z-dependent colloid density profile is obtained as

$$\rho_c(z) = \rho_c^0 \exp\{-\beta[\varphi_c(z) + \mu_c^{ex}(z) - \mu_c^{0,ex}]\} \quad (43)$$

The coupled equations eqs 41 and 43 are solved iteratively.

References and Notes

(1) For a recent overview, see Poon, W. C. K. *J. Phys.: Condens. Matter* **2002**, *14*, R859.
(2) See, e.g.: Likos, C. N. *Phys. Reports* **2001**, *348*, 267.
(3) For a recent comparison between theoretical predictions and experimental data, see: Bolhuis, P. G.; Louis, A. A.; Hansen, J. P. *Phys. Rev. Lett.* **2002**, *89*, 128302. Ramakrishnan, S.; Fuchs, M.; Schweizer, K. S.; Zukoski, C. F. *J. Chem. Phys.* **2002**, *116*, 2201.
(4) Aarts, D. G. A. L.; van der Wiel, J. H.; Lekkerkerker, H. N. W. *J. Phys.: Condens. Matter* **2003**, *15*, 5245.
(5) For a review, see Brader, J. M.; Evans, R.; Schmidt, M. *Mol. Phys.* **2003**, *101*, 3349.
(6) Aarts, D. G. A. L.; Dullens, R. P. A.; Lekkerkerker, H. N. W.; Bonn, D. *J. Chem. Phys.* **2004**, *120*, 1973.
(7) Aarts, D. G. A. L.; Schmidt, M.; Lekkerkerker, H. N. W. *Science* **2004**, *304*, 847.
(8) Brader, J. M.; Dijkstra, M.; Evans, R. *Phys. Rev. E* **2001**, *63*, 041405.
(9) Brader, J. M.; Evans, R.; Schmidt, M.; Löwen, H. *J. Phys.: Condens. Matter* **2002**, *14*, L1.
(10) Wessels, P. P.; Schmidt, M.; Löwen, H. *J. Phys.: Condens. Matter* **2004**, *16*, L1.
(11) Brader, J. M.; Evans, R. *Europhys. Lett.* **2000**, *49*, 678.
(12) Moncho-Jordá, A.; Rotenberg, B.; Louis, A. A. *J. Chem. Phys.* **2003**, *119*, 12667.
(13) Asakura, S.; Oosawa, F. *J. Chem. Phys.* **1954**, *22*, 1255 and *J. Polym. Sci.* **1958**, *33*, 183.
(14) Vrij, A. *Pure Appl. Chem.* **1976**, *48*, 471.
(15) Bolhuis, P. G.; Louis, A. A.; Hansen, J. P.; Meijer, E. J. *J. Chem. Phys.* **2001**, *114*, 4296.
(16) Bolhuis, P. G.; Louis, A. A. *Macromolecules* **2002**, *35*, 1860.
(17) Rosenfeld, Y. *Phys. Rev. Lett.* **1989**, *63*, 980.
(18) Schmidt, M.; Löwen, H.; Brader, J. M.; Evans, R. *Phys. Rev. Lett.* **2000**, *85*, 1934.
(19) Louis, A. A. *J. Phys: Condens. Matter* **2002**, *14*, 9187.
(20) Louis, A. A.; Bolhuis, P. G.; Hansen, J. P.; Meijer, E. J. *J. Chem. Phys.* **2002**, *116*, 10547.
(21) Dijkstra, M.; Brader, J. M.; Evans, R. *J. Phys.: Condens. Matter* **1999**, *11*, 10079.
(22) Rotenberg, B.; Dzubiella, J.; Hansen, J. P.; Louis, A. A. *Mol. Phys.* **2004**, *102*, 1.
(23) Meijer, E. J.; Frenkel, D. *J. Chem. Phys.* **1994**, *100*, 6873.
(24) Louis, A. A.; Bolhuis, P. G.; Meijer, E. J.; Hansen, J. P. *J. Chem. Phys.* **2002**, *117*, 1893.
(25) Tang, Z.; Scriven, L. E.; Davis, H. T. *J. Chem. Phys.* **1991**, *95*, 2659.
(26) Roth, R.; Evans, R.; Lang A.; Kahl, G. *J. Phys.: Condens. Matter* **2002**, *14*, 12063; Yu, X. Y.; Wu, J. Z. *J. Chem. Phys.* **2002**, *117*, 10156.
(27) Sokolowski, S.; Fischer, J. *J. Chem. Phys.* **1992**, *96*, 5441.
(28) Chandler, D.; Weeks, J. D.; Andersen, H. C. *Science* **1983**, *220*, 4599.
(29) Wadewitz, T.; Winkelmann, J. *J. Chem. Phys.* **2000**, *113*, 1.
(30) Evans, R.; Brader, J. M.; Roth, R.; Dijkstra, M.; Schmidt, M.; Löwen, H. *Philos. Trans. R. Soc. London A* **2001**, *359*, 961.
(31) Dijkstra, M.; van Roij, R. *Phys. Rev. Lett.* **2002**, *89*, 208303−1.
(32) Hansen, J. P.; McDonald, I. R. *Theory of Simple Liquids*, 2nd ed.; Academic Press: London, U.K., 1986.